Neurobiology of Aging xxx (2017) 1–9

Contents lists available at ScienceDirect

Neurobiology of Aging

journal homepage: www.elsevier.com/locate/neuaging

Low-frequency oscillations in default mode subnetworks are associated with episodic memory impairments in Alzheimer's disease

Michele Veldsman [a,b,*], Natalia Egorova [b,c], Baljeet Singh [d], Dan Mungas [d], Charles DeCarli [d], Amy Brodtmann [b,c]

[a] Nuffield Department of Clinical Neurosciences, University of Oxford, John Radcliffe Hospital, Oxford, UK
[b] Behavioural Neuroscience and Stroke Divisions, Florey Institute for Neuroscience and Mental Health, Melbourne, Australia
[c] Melbourne Brain Centre, University of Melbourne, Parkville, Melbourne, Australia
[d] Department of Neurology and Center for Neuroscience, University of California at Davis, Davis, California, USA

ARTICLE INFO

Article history:
Received 8 February 2017
Received in revised form 25 July 2017
Accepted 29 July 2017

Keywords:
Alzheimer's disease
Episodic memory
Default mode network

ABSTRACT

Disruptions to functional connectivity in subsystems of the default mode network are evident in Alzheimer's disease (AD). Functional connectivity estimates correlations in the time course of low-frequency activity. Much less is known about other potential perturbations to this activity, such as changes in the amplitude of oscillations and how this relates to cognition. We examined the amplitude of low-frequency fluctuations in 44 AD patients and 128 cognitively normal participants and related this to episodic memory, the core deficit in AD. We show higher amplitudes of low-frequency oscillations in AD patients. Rather than being compensatory, this appears to be maladaptive, with greater amplitude in the ventral default mode subnetwork associated with poorer episodic memory. Perturbations to default mode subnetworks in AD are evident in the amplitude of low-frequency oscillations in the resting brain. These disruptions are associated with episodic memory demonstrating their behavioral and clinical relevance in AD.

1. Introduction

Changes in default mode network (DMN) connectivity are implicated in the pathophysiological changes and episodic memory impairments that are hallmarks of Alzheimer's disease (AD) (Greicius et al., 2004; Hedden et al., 2009; Zhang and Raichle, 2010). The task-negative intrinsic network (Raichle et al., 2001) is thought to reflect self-referential and memory-related processing. Key nodes of the DMN, including the posterior cingulate, precuneus and medial temporal lobes show atrophy, hypometabolism, and hypoperfusion in the progression of AD (Braskie and Thompson, 2013; Chetelat et al., 2003). Disruptions to the DMN, as measured by functional connectivity, are evident both preclinically and with disease progression (Damoiseaux et al., 2012; Greicius et al., 2004; Petrella et al., 2011; Sheline and Raichle, 2013).

Functional connectivity is typically estimated by examining correlations in the time course of spontaneous low-frequency activity across the brain. This connectivity appears to reflect long-distance synchronous network activity, is highly reliable (Biswal et al., 2010), and functionally specific (Smith et al., 2009). When functional connectivity is estimated in this way, the DMN fractionates into subnetworks composed of anterior, ventral, and posterior nodes, each subserving different cognitive functions (Andrews-Hanna et al., 2010; Whitfield-Gabrieli et al., 2011). For example, the anterior DMN (aDMN) is associated with self-referential thought and decision-making, while the posterior network is more associated with familiarity and autobiographical memory (Damoiseaux et al., 2012). The ventral network (sometimes called the medial temporal lobe subsystem) is the subnetwork most closely associated with episodic memory, which is especially vulnerable to impairment in AD (Andrews-Hanna et al., 2010; Jones et al., 2015).

The DMN subnetworks are not uniformly disrupted in AD (Jones et al., 2015). The posterior DMN (pDMN) often shows hypoconnectivity while the anterior and ventral networks show hyperconnectivity (Damoiseaux et al., 2012; Jones et al., 2015). Posterior

* Corresponding author at: Nuffield Department of Clinical Neurosciences, University of Oxford, John Radcliffe Hospital, Level 6, West Wing, Oxford OX3 9DU, UK. Tel.: +44 07908090888; fax: +44 1865234632.
E-mail address: michele.veldsman@ndcn.ox.ac.uk (M. Veldsman).

0197-4580/$ – see front matter © 2017 Elsevier Inc. All rights reserved.
http://dx.doi.org/10.1016/j.neurobiolaging.2017.07.011

DMN hypoconnectivity is a robust finding detected early in the course of AD (Jones et al., 2015). The hyperconnectivity of the anterior and ventral default mode subnetworks may reflect compensatory activity as a result of posterior network amyloid beta (Aβ) deposition (Mormino et al., 2011). However, recent evidence suggests hyperconnectivity is not compensatory but instead reflects the shift of burden, as a result of early posterior network failures, to the anterior and ventral systems (Jones et al., 2015). Hyperconnectivity is therefore maladaptive, creating overload in the anterior and ventral networks and a metabolic burden that results in a cascade of network failures (Jones et al., 2015). The precise mechanisms behind this cascading network failure have yet to be elucidated. This may be in part to reliance in the field on examining correlations in the time course of activity to estimate functional networks.

Considerably less attention has been given to the amplitude of spontaneous low-frequency activity (Zuo et al., 2010). Although limited, there is emerging evidence of a relationship between low-frequency oscillations (LFOs) and functional connectivity that warrants further investigation (Di et al., 2013; Mascali et al., 2015; Weiler et al., 2014). The amplitude and fractional amplitude of low-frequency fluctuations (ALFF and fALFF, respectively) are reliable, reproducible (Zou et al., 2008; Zuo et al., 2010), and have a sensitivity capable of revealing intrinsic network disruption between clinical groups (Han et al., 2011; He et al., 2007; Yu-Feng et al., 2007). Several lines of evidence suggest that the amplitude of spontaneous LFO may be a useful clinical marker of network disruption in AD. The amplitude of LFOs is highest within the posterior cingulate and medial prefrontal cortex (Ghosh et al., 2008; Zou et al., 2008; Zuo et al., 2010), key regions of the DMN which show hypometabolism, and Aβ deposition in AD. The amplitude of LFOs also has behavioral relevance, showing modulation with task performance (Zuo et al., 2010). Studies have examined ALFF in mild cognitive impairment (MCI) and AD and shown disruption to LFOs in regions including the posterior cingulate and precuneus, with amplitudes decreasing with disease progression, examined cross-sectionally (Liang et al., 2014). These studies have primarily used ALFF as the measure of LFOs and reported both increases and decreases in amplitude in AD compared to healthy controls, depending on the region examined (Liu et al., 2014; Weiler et al., 2014). Importantly, the regions implicated frequently include known DMN nodes such as the posterior cingulate, precuneus, hippocampus, and parahippocampus (Liu et al., 2014; Weiler et al., 2014). In amnestic mild cognitive impairment (aMCI), which many researchers regard as preclinical AD, the amplitude of LFOs are reduced in many regions of the DMN, depending on the frequency band that is examined (Han et al., 2011). Research in aMCI, and other clinical populations, including schizophrenia and stroke, suggests that disruptions to LFOs are frequency dependent (Han et al., 2011; La et al., 2016; Zuo et al., 2010). For example, disruptions to LFO amplitudes in DMN hub, the posterior cingulate, are greater in the slow 5 band than in the slow 4 band in aMCI (Han et al., 2011). Frequency-dependent alterations in LFO have been investigated in AD, using ALFF but not fALFF, and have also shown different patterns of disruption in the slow 5 band compared with the slow 4 band (Liu et al., 2014). This suggests that disruptions to LFOs in AD are region and frequency band specific.

We examined the fALFF in AD patients compared to cognitively normal (CN), controls across the full low-frequency band (0.01–0.1 Hz) and the slow 4 (0.027–0.073 Hz) and slow 5 (0.01–0.027 Hz) frequency bands. The slow 4 and slow 5 bands have been shown to be more sensitive to signal from gray matter (GM; Zuo et al., 2010) but also show differential patterns of disruption in aging and clinical populations (Han et al., 2011; La et al., 2016). The amplitude of LFOs may be decreased in AD patients, reflecting hypoactivation; increased, reflecting hyperactivation; or some combination of the hyperactivation and hypoactivation, as is seen in the connectivity of DMN subnetworks derived from correlations in the time course of activity across the brain. To investigate whether LFO amplitude changes in AD have behavioral and clinical relevance, we examined the relationship between episodic memory performance, a core deficit in AD, and the amplitude of LFOs in default mode subnetworks. We hypothesized that episodic memory performance would be most closely associated with the amplitude of LFOs in the ventral DMN (vDMN) subnetwork because of its association with episodic memory, the core deficit of AD (Andrews-Hanna et al., 2010; Jones et al., 2015). Again, this relationship may be positive, reflecting compensatory rises in amplitude to maintain performance, or negative, reflecting a maladaptive overload of the network that does not benefit performance.

2. Materials and methods

2.1. Participants

Data from 44 patients and 128 CN volunteers were analyzed (see Table 1 for participant demographics). Participants received a comprehensive, multidisciplinary clinical evaluation at the Alzheimer's Disease Center, UC Davis. The study was approved by the UC Davis Institutional review board, and participants provided written informed consent to participate. Participants underwent a neuropsychological battery as well as detailed medical history and physical and neurological examination. Participants were assigned to the CN control group if they showed no signs of cognitive impairment (scored greater than −1.5 standard deviations (SDs) from the age- and education-adjusted means in cognitive testing). Diagnosis of AD was made according to the standardized criteria and methods (Morris et al., 2006). To ensure group differences were not driven by vascular burden, the presence and number of vascular risk factors (e.g., hypertension, diabetes, or hyperlipidemia) were recorded for each participant based on a thorough review of their medical history, medical records, and medications at the time of initial evaluation. A history of coronary artery disease (angina, coronary stent, coronary artery bypass graft surgery, and

Table 1
Participant demographics

	Cognitively normal	AD patients	Group difference (p)
Gender (male/female)	40/88	22/22	
Mean age (SD)	74.6 (6.1)	78.0 (8.7)	0.02*
Mean years of education (SD)	13.5 (8.9)	13.1 (4.8)	0.69
Median vascular risk	0.17 (0.1)	0.17 (0.1)	0.50
Mean episodic memory composite Z-score	0.13 (0.8)	−1.51 (0.5)	0.001**
Mean executive memory composite Z-score	0.12 (0.6)	−0.96 (0.7)	0.001**
Mean semantic memory composite Z-score	0.34 (0.8)	−0.49 (0.9)	0.001**
Mean spatial memory composite Z-score	0.21 (0.8)	−0.38 (1.1)	0.01*
Mean GM volume (cm^3)	547 (50)	520 (47)	0.002*
Mean GM volume/ICV (SD)	0.48 (0.02)	0.45 (0.03)	0.001**
Mean normalized white matter hyperintensity volume cm^3 (SD)	11.22 (13.2)	11.26 (8.5)	0.98

Means compared with Welch's t test (2-tailed significance level reported).
Median vascular risk compared with Mann-Whitney U test.
Significant to $^{*}p < 0.05$, $^{**}p < 0.01$.
Key: AD, Alzheimer's disease; GM, gray matter; ICV, intracranial volume; SD, standard deviation.

myocardial infarction) or cerebrovascular disease (transient ischemic attack, carotid endarterectomy, or carotid stent) was assessed by a similar review. A vascular burden score was created for all participants based on the addition of vascular risk factors and vascular events. The score could vary from 0 to 5.

2.2. Imaging parameters

Imaging data were collected on a 1.5T GE Sigma Horizon LX Echospeed system (GE Healthcare, Waukesha, WI, USA) at the UC Davis Imaging Research Centre.

Echoplanar images were acquired for 8 minutes with 3-mm isotropic voxels (2000-ms repetition time [TR]; 40-ms echo time [TE]; 24, 5-mm thick slices; 90° flip angle and field of view [FOV]). Participants were not given any specific instructions during the resting-state scan. High-resolution T1-weighted 3D Fast Spoiled Gradient-Recalled Echo Sequence structural images were acquired with 1-mm isotropic voxels (TR 9 ms [minute]; TE 2.9 ms [minute]; 128, 1.5-mm thick slices, 15° flip angle; 25 cm × 25 cm FOV; and 256 × 256 matrix). A fluid-attenuated inversion recovery image was also acquired (TR 11,000 ms; TE 144 ms; inversion time 2250 ms; 3 mm thick slices, 90° flip angle; 22 cm × 22 cm FOV; and 256 [frequency] × 192 [phase] matrix).

2.3. Image processing

The T1-weighted Fast Spoiled Gradient-Recalled Echo images were segmented into GM, white matter (WM), and cerebrospinal fluid using an in-house implementation of a Bayesian maximum-likelihood expectation-maximization algorithm to compute voxel-level tissue classification (Dempster et al., 1977; Fletcher et al., 2012). Intracranial volume (ICV) was calculated as the total volume of the native-space, skull-stripped volume. To calculate ICV, first multiple atlas skull-stripping is performed using atlases aligned with nonrigid body registration to the T1 image. Using a simultaneous truth and performance level estimation procedure, the most likely ICV segmentation is then iteratively computed. White matter hyperintensities (WMHs) were segmented in the fluid-attenuated inversion recovery images using methods described in the study by He et al. (2012).

Functional images were preprocessed in SPM8 (Wellcome Department of Imaging Neuroscience, London, UK). Preprocessing included slice-time correction, six-parameter rigid body realignment to estimate and correct head motion, coregistration to the structural image, normalization to Montreal Neurological Institute template space, and smoothing with a 6-mm full-width at half maximum Gaussian kernel. Six-parameter motion regression estimates were used to calculate framewise displacement according to Power et al., who recommend a motion threshold of less than 0.5 mm (Power et al., 2012, 2014). Mean framewise displacement was not significantly different between the AD (mean 0.19, SD: 0.11) and CN control group (mean 0.19, SD: 0.14) when compared using a 2 sample t test $t(170) = 0.34$, $p = 0.74$.

Normalized and smoothed functional images were imported into the resting-state fMRI data analysis toolkit (REST) toolbox (Song et al., 2011) for further processing, including linear trend removal. Time series data were transformed to frequency domain, and the power spectrum was calculated using fast Fourier transform functions implemented in the REST toolbox (Song et al., 2011). The amplitude of LFOs can be estimated using ALFF, a measure of the total power in a given frequency range, or fALFF, the total power in the given frequency range as a fraction of total power in the entire detectable frequency range (Zuo et al., 2010). ALFF has shown somewhat better test-retest reliability than fALFF, but both measures show moderately high test-retest reliability (Zuo et al., 2010). fALFF additionally has higher specificity in GM and importantly higher specificity in the DMN than ALFF (Zuo et al., 2010). fALFF was developed as an improvement to ALFF (Zou et al., 2008) which is sensitive to physiological noise. fALFF is recommended over ALFF until better methods are developed to account for physiological noise (Zuo and Xing, 2014). fALFF was calculated as the ratio of the power in the full low-frequency range (0.01–0.08 Hz), the slow 5 range (0.01–0.027 Hz), and the slow 4 range (0.027–0.073 Hz) to the power in the full frequency range (0–0.25 Hz) (Zou et al., 2008) across every voxel in the brain (Zuo et al., 2010). Individual subject fALFF maps were normalized by dividing the fALFF value in each voxel by the global average fALFF value and exported to SPM8 for group-level analysis.

2.3.1. Default mode subnetwork region of interest analysis

Regions of interest were created in MARSeille Boîte À Région d'Intérêt (Brett et al., 2002) as 8-mm spheres around the peak coordinates (see Table 2) of the anterior, ventral, and posterior DMNs reported by Damoiseaux et al. (2012). We selected only regions of the subnetworks that were reported as showing either a significant change in AD patients over time, or a significant group interaction (CN compared to AD) in the study by Damoiseaux et al. (2012); that is, regions of the DMN that had direct relevance to AD. We excluded 2 regions that, on inspection, fell in cerebral WM.

2.4. Neuropsychological testing

Memory was assessed with Spanish and English neuropsychological assessment Scales (SENAS). The SENAS is designed to be psychometrically matched across English and Spanish versions. It is also psychometrically matched in its subscales and is specifically designed for use in aging populations (Mungas et al., 2004). The SENAS is designed to test conceptual thinking, semantic memory, attention span, episodic memory, nonverbal spatial abilities, and verbal abilities (Mungas et al., 2004). We chose to focus on the episodic memory component, as episodic memory impairment is a core deficit in AD. The episodic memory composite score is the

Table 2
Default mode subnetwork regions of interest

Default mode subnetwork	Region of interest	Hemisphere	MNI coordinates		
			x	y	z
Anterior	Superior frontal gyrus	R	20	24	56
	Lateral occipital cortex	L	−52	−72	20
	Inferior temporal gyrus	R	54	−2	−42
	Lateral occipital cortex	R	46	−80	−6
	Precentral gyrus	R	60	−6	46
	Superior frontal gyrus	R	20	26	56
Posterior	Middle temporal gyrus (posterior)	L	−66	−50	2
	Middle temporal gyrus	R	56	−32	−2
	Middle temporal gyrus (anterior)	L	−60	−28	−6
	Middle temporal gyrus	L	−62	−12	−12
	Superior frontal gyrus	L	−4	44	42
	Supramarginal gyrus	R	60	−38	12
	Planum temporale	R	36	−36	18
Ventral	Inferior frontal gyrus	L	−36	16	20
	Lingual gyrus	L	−6	−56	0
	Cuneal cortex	R	10	−84	40
	Middle frontal gyrus	R	40	20	24
	Paracingulate gyrus	R	10	54	−4
	Precuneus cortex	R	18	−56	6
	Postcentral gyrus	L	−2	−42	68
	Lingual gyrus	R	8	−40	−4
	Lateral occipital cortex	R	10	−84	42

8-mm spheres created around the peak of activation reported in Damoiseaux et al. (2012). Coordinates reported in Montreal Neurological Institute (MNI) template space.

average of 2 word-list tasks (Word List Learning I and II) measuring learning and delayed recall.

2.5. Statistical analysis

Normalized GM volumes, WMH loads, and age were included as nuisance covariates in the voxelwise regressions at the group level for the full range, slow 5 and slow 4 analyses separately, in SPM8. Normalized values from the individual fALFF maps were extracted from all regions of interest (ROIs) using the REST toolbox. We excluded one control participant from all imaging analyses. The outlier control participant had normalized amplitudes in a number of ROIs that were significantly higher (greater than 3 SDs) than the rest of the group. Inclusion of this subject drove correlations to significance, but it was clear the effect was driven by the extreme value. Amplitudes across ROIs within each subnetwork were averaged and compared in a repeated measures analysis of variance with frequency band (slow 5 and slow 4) and network (aDMN, pDMN, and vDMN) as within subject factors and group (AD, CN) as a between-subject factor. Post hoc comparisons were made with Welch's independent sample t tests which are more robust to unequal sample size and variance between groups (Ruxton, 2006). Normalized episodic memory scores were correlated with amplitudes extracted from subnetwork ROIs across all participants (patients and controls). Bonferroni correction was used to account for multiple comparisons in all statistical tests. All statistics were carried out in JASP software (Love et al., 2015). The threshold for statistical significance was set at $p < 0.05$ except where correction for multiple comparisons was necessary (false discovery rate in the voxelwise analysis and Bonferonni correction in ROI and correlation analyses).

3. Results

In terms of group demographics (see Table 1), AD patients and CN controls were well matched in the number of years of education and vascular risk score. AD patients were significantly older than CN controls and scored significantly lower on the SENAS episodic memory component score.

3.1. Voxelwise analysis in different frequency bands

In the full frequency range (0.01–0.1 Hz), fALFF revealed a clear DMN in CN controls, with amplitudes highest in the posterior cingulate—a major hub of the DMN. In AD, this network was less widespread and reduced in the precuneus and posterior cingulate. A direct contrast of the CN and AD groups showed greater amplitudes of LFOs in the posterior DMN in the CN group compared to AD patients. The reverse contrast showed no regions with significantly higher amplitudes in AD compared to CN controls that survived a threshold corrected for multiple comparisons (height threshold $p <$ 0.05 false discovery rate corrected).

In the slow 5 frequency range (0.01–0.027 Hz), CN controls and AD patients exhibited greater anterior and ventral DMN involvement than in the full or the slow 4 range. Regions of the anterior and ventral DMN, including the precentral and postcentral gyrus, showed higher amplitudes in the slow 5 range in AD patients compared to CN controls. The reverse contrast showed higher amplitudes in the CN group in a small region on the brainstem only (Supplementary 1, Fig. 1B).

In the slow 4 range (0.027–0.073 Hz), in line with previous research, slow 4 amplitudes were dominant in midline regions (Zuo et al., 2010) in CN controls with lateral temporal, medial temporal, and paracingulate components of the vDMN evident. In the AD group, ventral and posterior DMN components were evident including the posterior cingulate, cuneus, and postcentral gyrus and also showed greater amplitudes compared to CN controls. The temporal poles and regions within WM showed higher amplitudes in CN controls than in AD patients (Supplementary Material 1, Fig. 1A). fALFF has been shown to have high specificity to GM, and although amplitudes are overall higher in GM, there is some noise from WM sources. This is greater when LFOs are estimated with ALFF (Zuo et al., 2010).

A qualitative comparison of the spatial distribution of LFOs in CN controls in the full band (Fig. 1, row 1A), the slow 4 (Fig. 1, row 3A), and the slow 5 (Fig. 1, row 2A) bands suggest that the full band in CN controls is dominated by amplitudes in the slow 5 (0.01–0.027 Hz) range. The spatial distribution of LFOs in the AD group differed between the slow 4 (Fig. 1, row 3B) and slow 5 bands (Fig. 1, row 2B), with the slow 5 band showing medial frontal anterior components of the DMN not evident in the slow 4 band.

3.2. ROI analysis

A repeated measures analysis of variance with frequency band (slow 5 and slow 4), network (aDMN, pDMN, and vDMN) and group as factors (AD, CN) revealed a significant main effect of network ($f(1,169) = 377.95$, $p < 0.001$, $\eta^2_p = 0.69$), frequency band ($f(1,169) = 57.24$, $p < 0.001$, $\eta^2_p = 0.25$), and group ($f(1,169) = 24.43$, $p < 0.001$, $\eta^2_p = 0.13$) on amplitude of LFOs. The AD group had higher overall amplitude of LFOs compared to CN controls, $p < 0.001$. Amplitude was higher in the slow 4 compared to the slow 5 band, $p < 0.001$. Average amplitude was significantly lower in the anterior compared to the posterior DMN, $p < 0.001$, which was significantly lower than the ventral DMN, $p < 0.001$ (all post hoc tests Bonferroni corrected). There was a significant interaction between network and group ($f(1,169) = 3.15$, $p < 0.05$, $\eta^2_p = 0.006$) and frequency band and network ($f(1,169) = 41.91$, $p < 0.001$, $\eta^2_p = 0.20$). We used Welch's independent samples t tests to further probe the key interaction between network and group (Table 3). In the slow 5 band, there were no significant group differences in amplitudes across the ROIs in all networks. In the slow 4 band, there were significant group differences with greater amplitudes in the middle temporal gyrus of the pDMN and the cuneal cortex and lateral occipital cortex of the vDMN in AD.

3.3. Relationship with episodic memory

To test the behavioral and clinical significance of altered LFOs, we correlated amplitude of LFOs in key DMN subnetwork regions with episodic memory across the entire group of CN controls and AD patients and across the AD group only (Table 3). Only the slow 4 frequency band showed significant group differences in amplitudes between AD patients and CN controls. Therefore, we restricted correlations to amplitudes within the slow 4 frequency band. As is evident in Table 3, after correcting for multiple comparisons, significant correlations were observed in the cuneal cortex, the paracingulate gyrus, and the lateral occipital cortex of the vDMN across the whole group. These correlations were negative, indicating that increased amplitudes were associated with lower episodic memory scores in these regions (Table 3 and Fig. 2).

4. Discussion

The DMN is the core intrinsic network implicated in AD, with episodic memory deficits reflecting a core clinical feature. Most studies investigating the involvement of the DMN in AD have focused on the spatial distribution of correlations in the time course of spontaneous activity within the network, and the evidence is mixed as to the specific clinical and functional significance of

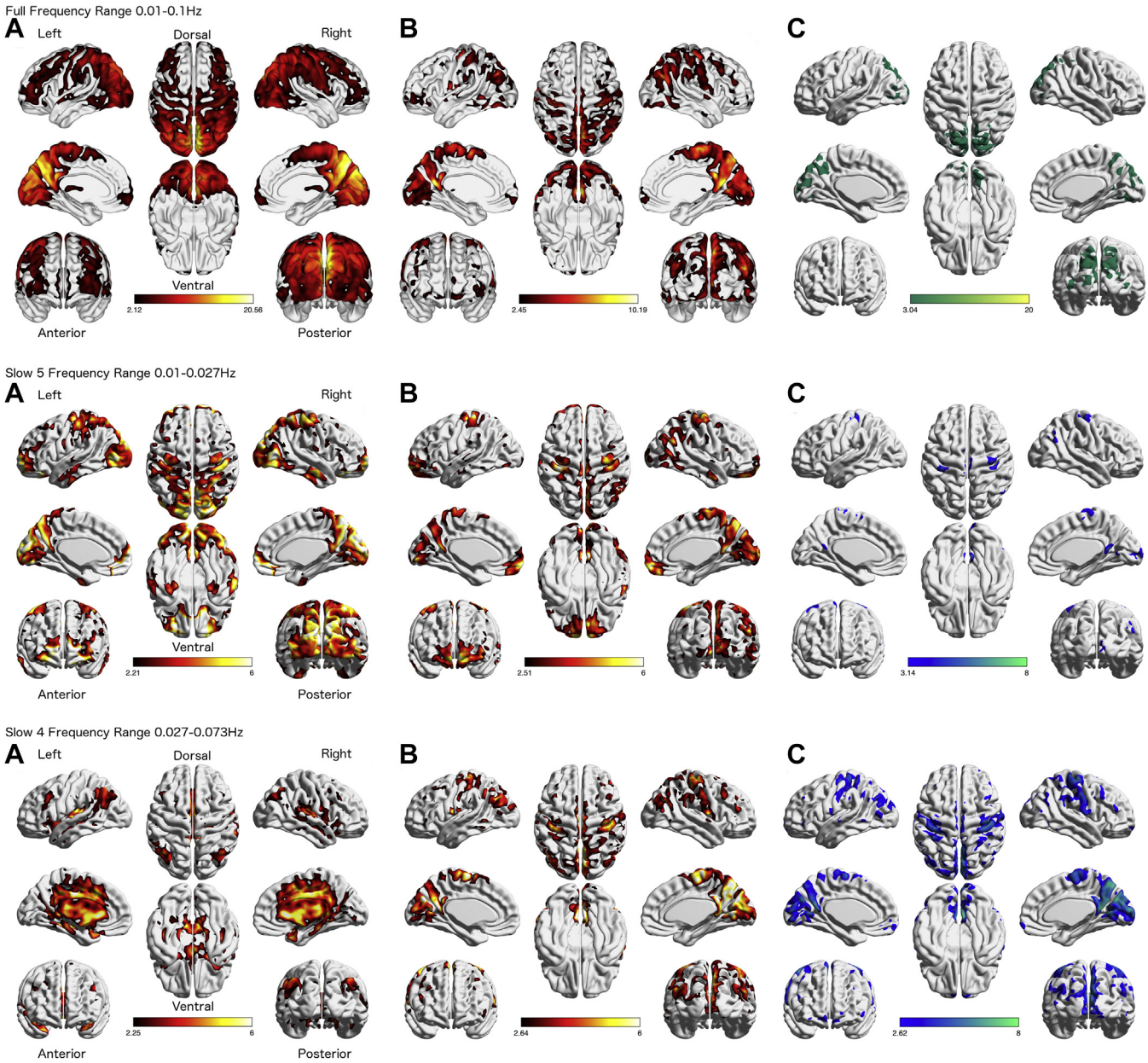

Fig. 1. Fractional amplitude of low-frequency fluctuations in the full frequency range in row 1 (A) cognitively normal (CN) controls, (B) AD patients, (C) group difference showing significantly greater fALFF in CN compared to AD patients. fALFF in the slow 5 frequency band in row 2 and the slow 4 band in row 3 in (A) CN controls, (B) AD patients and (C) group difference showing AD greater than CN. False discovery rate height corrected to *p*.

default mode subnetwork disruption. Here, we explored the amplitude of LFOs in default mode subnetworks and related this to episodic memory performance.

In the 0.01–0.1 Hz frequency range, we showed the amplitude of spontaneous LFOs in the resting brain was highest in the posterior cingulate, the major hub of the DMN. Hypometabolism and Aβ deposition in the posterior cingulate is an early marker of AD (Braskie and Thompson, 2013; Chetelat et al., 2003). LFOs may therefore have clinical relevance as a marker of intrinsic network disruption in AD. The posterior cingulate is the core of the pDMN. When estimated as temporal correlations in spontaneous activity, the pDMN is first of the DMN subnetworks to show hypo-connectivity preclinically (Binnewijzend et al., 2012) that increases with the progression of AD (Jones et al., 2015). Here, we extend this finding to show lower amplitude of LFOs in key regions of the posterior DMN including the posterior cingulate and precuneus.

Functional connectivity estimated as the spatial distribution of temporal correlations typically focuses on the 0.01–0.1 Hz frequency band, the full frequency range examined here. There is increasing evidence that clinically relevant information exists within the amplitudes of the different frequency bands, including those below 0.1 Hz (Han et al., 2011; La et al., 2016; Zuo et al., 2010). In the current study, the spatial distribution of amplitudes in the slow 5 band suggested that LFOs in the full range are dominated by 0.01–0.27 Hz frequencies in CN controls. In line with our voxelwise findings in CN controls, the peak of the distribution of frequencies at 0.01–0.1 Hz is below 0.3 Hz (La et al., 2016), and slow 4 amplitudes are concentrated in midline, basal ganglia, and thalamic

Table 3
Group differences between AD patients and CN controls (negative values indicate higher amplitudes in CN)

Default mode subnetwork	Region of interest	Group difference				Whole group correlation with episodic memory		AD group correlation with episodic memory	
		Slow 5		Slow 4		r	*p*-value	r	*p*-value
		Cohen's D	*p*-value	Cohen's D	*p*-value				
Anterior	Superior frontal gyrus	0.03	0.90	0.25	0.20	−0.14	0.08	−0.00	0.99
	Lateral occipital cortex	0.36	0.08	0.68	0.003	−0.17	0.03	0.14	0.40
	Inferior temporal gyrus	0.07	0.74	−0.22	0.29	0.06	0.42	−0.11	0.53
	Lateral occipital cortex	0.28	0.23	0.17	0.40	−0.10	0.19	−0.01	0.94
	Precentral gyrus	0.25	0.24	0.61	0.003	−0.23	0.003	0.04	0.82
	Superior frontal gyrus	0.04	0.85	0.18	0.38	−0.13	0.11	−0.02	0.89
Posterior	Middle temporal gyrus (posterior)	0.30	0.13	0.64	0.001	−0.22	0.004	−0.20	0.24
	Middle temporal gyrus	−0.08	0.70	−0.12	0.57	−0.03	0.71	−0.03	0.87
	Middle temporal gyrus (anterior)	−0.11	0.57	0.32	0.12	−0.17	0.03	−0.10	0.55
	Middle temporal gyrus	0.22	0.25	0.27	0.18	−0.15	0.07	−0.18	0.29
	Superior frontal gyrus	−0.02	0.94	−0.17	0.40	0.13	0.11	0.27	0.11
	Supramarginal gyrus	0.35	0.09	−0.04	0.85	−0.05	0.52	0.14	0.40
	Planum temporale	−0.24	0.26	0.09	0.71	−0.01	0.86	−0.00	0.96
Ventral	Inferior frontal gyrus	−0.23	0.29	−0.08	0.72	0.03	0.68	−0.03	0.87
	Lingual gyrus	0.45	0.06	0.60	0.01	−0.23	0.004	−0.01	0.97
	Cuneal cortex	0.24	0.27	1.15	0.001[a]	−0.27	0.001[a]	0.04	0.84
	Middle frontal gyrus	−0.28	0.16	0.06	0.80	−0.03	0.72	0.06	0.72
	Paracingulate gyrus	0.30	0.16	0.43	0.01	−0.26	0.001[a]	−0.35	0.03
	Precuneus cortex	−0.11	0.63	0.24	0.29	−0.12	0.12	−0.06	0.74
	Postcentral gyrus	0.56	0.01	0.63	0.007	−0.10	0.19	0.15	0.37
	Lingual gyrus	0.06	0.80	−0.23	0.31	0.06	0.49	−0.01	0.98
	Lateral occipital cortex	0.31	0.15	1.20	0.001[a]	−0.28	0.001[a]	0.05	0.77

Correlation between normalized episodic memory scores and amplitude in the slow 4 frequency band in default mode subnetwork regions of interest. Pearson's correlation coefficient reported.
Key: AD, Alzheimer's disease; CN, cognitively normal.
[a] Significant at Bonferroni corrected $p < 0.001$; ($p < 0.05/44$ tests).

regions (Zuo et al., 2010). This peak seems to shift to a higher frequency with age and after stroke (La et al., 2016). These subcortical regions may be the generators of slow 4 LFOs. Converging evidence from neuron recording in awake rats shows the basal ganglia, in particular, as the source of spontaneous slow 4 oscillations (Zuo et al., 2010). This lends further weight to a neural source of LFOs. One of our most striking findings was the higher amplitude in AD patients in regions of the posterior and ventral DMN in the higher frequency slow 4 band in AD patients when compared to the CN group. This mirrors findings in a subacute stroke population where an increase in amplitude in the slow 4 band relative to healthy controls was reported (La et al., 2016). Some of the posterior components seen in the study by La et al. (2016) overlap with the same regions that showed lower amplitudes in the full range of our LFO analysis, suggesting that these regions may be vulnerable to disruption in clinical populations. This also highlights the importance of examining different frequency bands, as frequency-specific disruptions to DMN subnetworks can manifest as increased or decreased amplitude (Han et al., 2011). Liu et al. (2014) also demonstrated frequency-specific effects in a group of 23 patients with moderate AD and 27 age-match controls using ALFF. In contrast to the results presented here, they show decreased ALFF in the posterior components of the DMN in AD. ALFF and fALFF have been shown to diverge within the same brain regions, with negative values (relative to global mean) seen in fALFF compared with positive values for ALFF (Zou et al., 2008). It is unclear whether the diverging results between our study and Liu et al. (2014) are due to our use of fALFF, compared with ALFF in their study, or characteristics of the groups studied. We chose to use fALFF on the basis that it has been shown to be more specific to LFOs derived from GM and less sensitive to physiological noise (Zou et al., 2008).

The subnetwork ROI analysis confirmed a different pattern of disruption in AD in the slow 5 and slow 4 frequency bands. The slow 4 band showed significant amplitude differences in middle temporal gyrus of the pDMN and the cuneus and lateral occipital cortex regions of the vDMN. In these regions, amplitude was greater in AD patients than CN controls, confirming the findings of voxelwise analysis. Within the vDMN and extending to a paracingulate region, higher amplitudes were associated with lower scores on the episodic memory component of the SENAS across the AD patients and CN controls. This key finding demonstrates the behavioral and clinical relevance of the slow 4 amplitude increases.

Increased connectivity of intrinsic network activity is variably interpreted, sometimes as compensatory and sometimes as evidence of network failure. The cascading network failure hypothesis predicts that hyperconnectivity would result from increased burden on the anterior and ventral subnetworks resulting from early posterior DMN failure. Our results are in line with this theory, with decreased posterior intrinsic network activity evident at the full range and greater amplitudes in the ventral and anterior default mode subnetworks in the slow 4 and slow 5 range. Importantly, our results reveal subnetwork disruptions when frequency-specific amplitude of LFOs were examined, as opposed to the more commonly investigated correlations in the time course of spontaneous activity. Our finding that amplitudes in vDMN subnetworks were negatively associated with episodic memory performance gives further weight and clinical relevance to the maladaptive nature of these amplitude increases since episodic memory performance is known to be associated with the ventral subsystem of the DMN in both task-based and resting-state functional magnetic resonance imaging (Damoiseaux et al., 2012; Jones et al., 2015). Further evidence of the potentially maladaptive nature of amplitude increases has been shown by Pasquini et al. (2016) who show

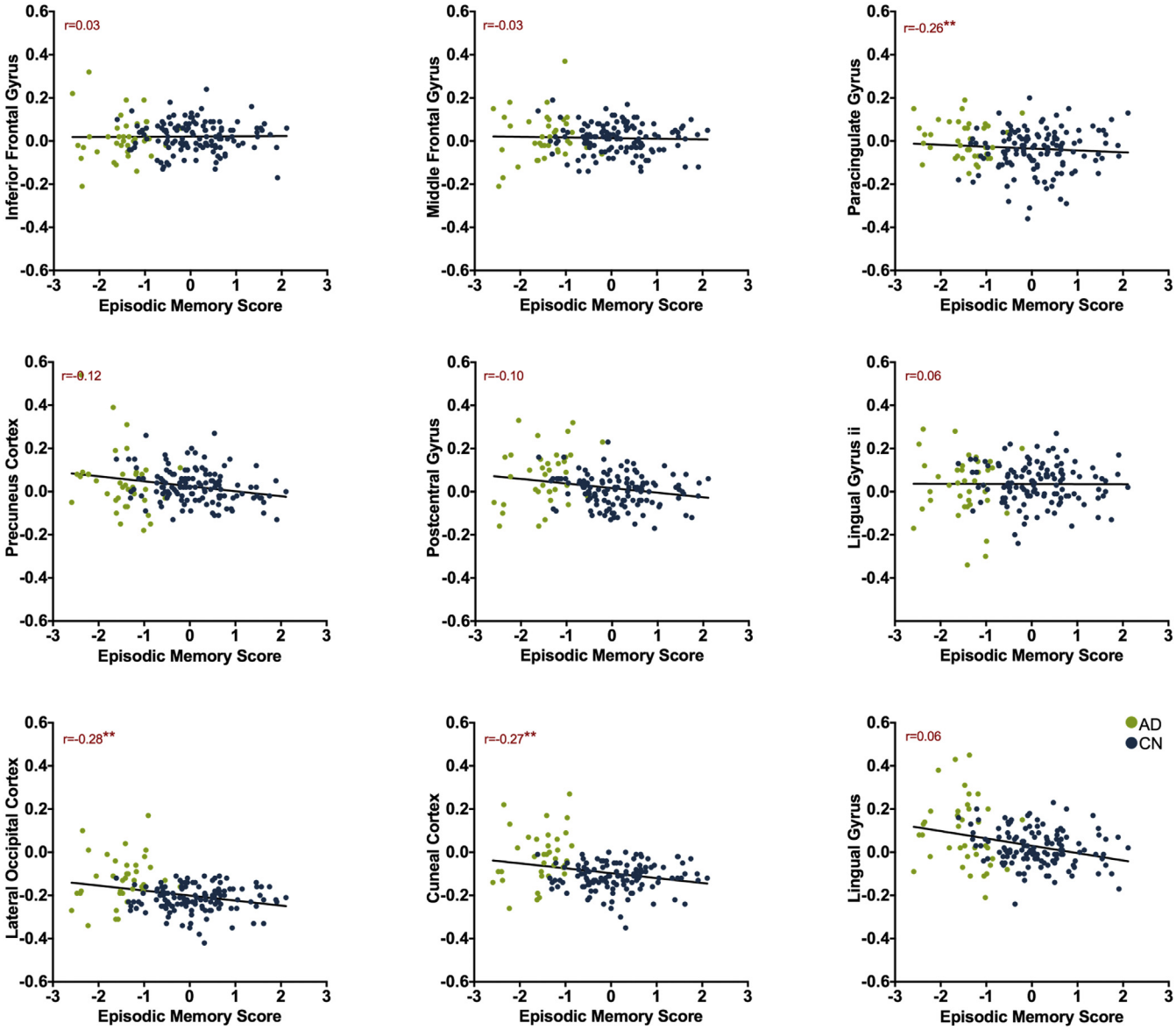

Fig. 2. Correlation between normalized episodic memory scores and slow 4 frequency range LFOs in ventral default mode subnetwork regions of interest. **Significant at Bonferroni corrected *p*.

increased amplitudes of LFOs in the medial temporal lobe associated with medial parietal cortical thinning in AD.

We have shown disrupted amplitude of LFOs in AD in regions of the DMN that are derived from functional connectivity measured as correlations in the time course of activity at rest. This calls into question the relationship between LFOs and functional connectivity. A number of studies in healthy controls and clinical populations, including MCI and AD, have noted the close spatial correspondence between the DMN functional network and the spatial profile of LFOs (Han et al., 2011; La et al., 2016; Zou et al., 2008; Zuo et al., 2010). Regions within the DMN, particularly the posterior cingulate, showing the highest amplitude of LFOs in the healthy resting brain show disruption in AD in both their connectivity to other DMN regions and the amplitude of LFOs (Jones et al., 2015; Weiler et al., 2014; Zou et al., 2008; Zuo et al., 2010). Although research into this relationship is in its infancy, there has also been more direct evidence of the relationship between connectivity and LFOs (Di et al., 2013; Mascali et al., 2015; Weiler et al., 2014). In a group of 29 controls, 20 aMCI and 32 AD patients, functional connectivity of the posterior cingulate was used to create a mask in which the amplitude of LFOs was examined. ALFF was correlated with functional connectivity of the posterior cingulate cortex and regions of the DMN (Weiler et al., 2014). Both ALFF and functional connectivity of the posterior cingulate cortex was reduced in AD leading the authors to speculate that the reduced intrinsic activity underlies functional connectivity (Weiler et al., 2014). This is highly speculative based on correlational data; nevertheless, the relationship between LFOs and connectivity was demonstrated. In a more thorough, systematic investigation of the relationship between functional connectivity and LFOs in 79 healthy older adults, Di et al. (2013) showed a correlation between ALFF and functional connectivity derived from both independent component analysis and region of interest–based analysis, including within the DMN (Di et al., 2013). The specificity of the correlations between ALFF and connectivity, that is, it was not a uniform whole brain phenomenon, led the authors to suggest that the associations have functional

significance (Di et al., 2013). They further posit that hub-like regions with strong functional connections, and therefore multiple inputs and outputs, have higher amplitudes associated with their greater overall neural activity (Di et al., 2013). This is in line with the functional connectivity network literature in which hub regions, which are highly metabolically active and highly interconnected, are disproportionately vulnerable to brain diseases, including neurodegenerative dementias (Fornito et al., 2015). In AD, the posterior cingulate is such a hub, showing amyloid deposition and hypometabolism early in disease onset (Fornito et al., 2015).

The origins of LFOs are not yet clear (Zuo et al., 2010). Regions that show spontaneous LFOs maybe be regions that are more susceptible to physiological noise, for example, due to proximity to large vessels (Di et al., 2013). However, there is good evidence to suggest LFOs reflect neural activity as opposed to vascular or respiratory fluctuations. LFO amplitudes show a high degree of test-retest reliability and specificity to GM (Zuo et al., 2010), correlate with neural activity recorded with electrocorticography (He et al., 2008), and are highest in regions with high levels of metabolic activity (Zhang and Raichle, 2010; Zuo et al., 2010). Reassuringly, oscillations seem to be robust to vascular contributions from breathing, even under conditions of breath holding (Zuo et al., 2010). We controlled for age, GM volume, and WMH load in our voxelwise analyses. Our group was also matched on vascular burden, suggesting that amplitude differences were not driven by vascular risk factors.

4.1. Limitations

A potential limitation of the study may be in the selection of ROIs to determine amplitude differences across DMN subnetworks. We limited the ROI selection to subnetwork regions relevant to AD or showing group differences based on Damoiseaux et al. (2012). However, we also included a whole brain voxelwise analysis that independently showed group differences within the default mode subnetworks. We also fully corrected all our ROI analyses to prevent false positives as a result of mass multiple hypothesis testing. Future work will clarify the fractionation of the DMN across frequency by examining amplitudes of LFOs in functional and structural parcellations across the brain. Correlations between resting-state networks and behavior suggest behavioral or clinical relevance of resting-state networks, but we cannot make any causal inferences on the relationship between behavior and intrinsic brain activity from these correlational findings alone. When examining correlations between episodic memory and fALFF in DMN subnetworks in the AD group alone, we did not find any significant correlations that survived correction for multiple comparisons. This may be because the range of memory scores in the AD group was limited (episodic memory impairment being at the core of AD diagnoses). The correlation across the group confirms that higher amplitude is associated with poorer episodic memory performance, but more direct evidence for the significance in AD would require the correlation to be replicated in the AD group alone. Finally, although we diagnosed AD according to comprehensive standardized criteria and methods (Morris et al., 2006), and took care to exclude cases driven by vascular pathology, we cannot completely rule out non-AD underlying pathologies in our AD group.

5. Conclusions

Disruptions to subsystems of the DMN are evident in the amplitude of spontaneous oscillations in the resting brain of Alzheimer's patients. Frequency-dependent amplitude of LFOs, measured with fALFF, in the ventral DMN is associated with lower episodic memory providing preliminary evidence of the clinical and behavioral importance of LFOs to intrinsic network function in AD.

Disclosure statement

The authors report no conflicts of interest.

Acknowledgements

The authors thank the patients and their families for donating their time to our research. This work was supported by the Collie Trust and Sidney and Fiona Myer Family Foundation.

Appendix A. Supplementary data

Supplementary data associated with this article can be found, in the online version, at http://dx.doi.org/10.1016/j.neurobiolaging.2017.07.011.

References

Andrews-Hanna, J.R., Reidler, J.S., Sepulcre, J., Poulin, R., Buckner, R.L., 2010. Functional-anatomic fractionation of the brain's default network. Neuron 65, 550–562.

Binnewijzend, M.A.A., Schoonheim, M.M., Sanz-Arigita, E., Wink, A.M., van der Flier, W.M., Tolboom, N., Adriaanse, S.M., Damoiseaux, J.S., Scheltens, P., van Berckel, B.N.M., Barkhof, F., 2012. Resting-state fMRI changes in Alzheimer's disease and mild cognitive impairment. Neurobiol. Aging 33, 2018–2028.

Biswal, B.B., Mennes, M., Zuo, X.-N., Gohel, S., Kelly, C., Smith, S.M., Beckmann, C.F., Adelstein, J.S., Buckner, R.L., Colcombe, S., Dogonowski, A.-M., Ernst, M., Fair, D., Hampson, M., Hoptman, M.J., Hyde, J.S., Kiviniemi, V.J., Kötter, R., Li, S.-J., Lin, C.-P., Lowe, M.J., Mackay, C., Madden, D.J., Madsen, K.H., Margulies, D.S., Mayberg, H.S., McMahon, K., Monk, C.S., Mostofsky, S.H., Nagel, B.J., Pekar, J.J., Peltier, S.J., Petersen, S.E., Riedl, V., Rombouts, S.A.R.B., Rypma, B., Schlaggar, B.L., Schmidt, S., Seidler, R.D., Siegle, G.J., Sorg, C., Teng, G.-J., Veijola, J., Villringer, A., Walter, M., Wang, L., Weng, X.-C., Whitfield-Gabrieli, S., Williamson, P., Windischberger, C., Zang, Y.-F., Zhang, H.-Y., Castellanos, F.X., Milham, M.P., 2010. Toward discovery science of human brain function. Proc. Natl. Acad. Sci. U. S. A. 107, 4734–4739.

Braskie, M.N., Thompson, P.M., 2013. Understanding cognitive deficits in Alzheimer's disease based on neuroimaging findings. Trends Cogn. Sci. 17, 510–516.

Brett, M., Anton, J.-L., Valabregue, R., Poline, J.-B., 2002. Region of interest analysis using the MarsBar toolbox for SPM 99. Neuroimage 16.

Chetelat, G., Desgranges, B., de la Sayette, V., Viader, F., Berkouk, K., Landeau, B., Lalevée, C., Le Doze, F., Dupuy, B., Hannequin, D., Baron, J.-C., Eustache, F., 2003. Dissociating atrophy and hypometabolism impact on episodic memory in mild cognitive impairment. Brain A. J. Neurol. 126, 1955–1967.

Damoiseaux, J.S., Prater, K.E., Miller, B.L., Greicius, M.D., 2012. Functional connectivity tracks clinical deterioration in Alzheimer's disease. Neurobiol. Aging 33, 828.e19–828.e30.

Dempster, A.P., Laird, N.M., Rubin, D.B., 1977. Maximum likelihood from incomplete data via the EM algorithm. J. R. Stat. Soc. Ser. B 39, 1–38.

Di, X., Kim, E.H., Huang, C.-C., Tsai, S.-J., Lin, C.-P., Biswal, B.B., 2013. The Influence of the amplitude of low-frequency fluctuations on resting-state functional connectivity. Front. Hum. Neurosci. 7, 118.

Fletcher, E., Singh, B., Harvey, D., Carmichael, O., Decarli, C., 2012. Adaptive image segmentation for robust measurement of longitudinal brain tissue change. In: Annual International Conference of the IEEE Engineering in Medicine and Biology Society, San Diego, CA.

Fornito, A., Zalesky, A., Breakspear, M., 2015. The connectomics of brain disorders. Nat. Rev. Neurosci. 16, 159–172.

Ghosh, A., Rho, Y., McIntosh, A.R., Kötter, R., Jirsa, V.K., 2008. Noise during rest Enables the Exploration of the Brain's Dynamic Repertoire. PLoS Comput. Biol. 4, e1000196.

Greicius, M.D., Srivastava, G., Reiss, A.L., Menon, V., 2004. Default-mode network activity distinguishes Alzheimer's disease from healthy aging: evidence from functional MRI. Proc. Natl. Acad. Sci. U. S. A. 101, 4637–4642.

Han, Y., Wang, J., Zhao, Z., Min, B., Lu, J., Li, K., He, Y., Jia, J., 2011. Frequency-dependent changes in the amplitude of low-frequency fluctuations in amnestic mild cognitive impairment: a resting-state fMRI study. Neuroimage 55, 287–295.

He, B.J., Snyder, A.Z., Zempel, J.M., Smyth, M.D., Raichle, M.E., 2008. Electrophysiological correlates of the brain's intrinsic large-scale functional architecture. Proc. Natl. Acad. Sci. U. S. A. 105, 16039–16044.

He, J., Carmichael, O., Fletcher, E., Singh, B., Iosif, A.-M., Martinez, O., Reed, B., Yonelinas, A., DeCarli, C., 2012. Influence of functional connectivity and structural MRI measures on episodic memory. Neurobiol. Aging 33, 2612–2620.

He, Y., Wang, L., Zang, Y., Tian, L., Zhang, X., Li, K., Jiang, T., 2007. Regional coherence changes in the early stages of Alzheimer's disease: a combined structural and resting-state functional MRI study. Neuroimage 35, 488–500.

Hedden, T., Van Dijk, K.R.A., Becker, J.A., Mehta, A., Sperling, R.A., Johnson, K.A., Buckner, R.L., 2009. Disruption of functional connectivity in clinically normal older adults harboring amyloid burden. J. Neurosci. 29, 12686–12694.

Jones, D.T., Knopman, D.S., Gunter, J.L., Graff-Radford, J., Vemuri, P., Boeve, B.F., Petersen, R.C., Weiner, M.W., Jack, C.R., 2015. Cascading network failure across the Alzheimer's disease spectrum. Brain 139, 547–562.

La, C., Nair, V.A., Mossahebi, P., Young, B.M., Chacon, M., Jensen, M., Birn, R.M., Meyerand, M.E., Prabhakaran, V., 2016. Implication of the Slow-5 oscillations in the disruption of the default-mode network in healthy aging and stroke. Brain Connect 6, 482–495.

Liang, P., Xiang, J., Liang, H., Qi, Z., Li, K. Alzheimer's Disease NeuroImaging Initiative, 2014. Altered amplitude of low-frequency fluctuations in early and late mild cognitive impairment and Alzheimer's disease. Curr. Alzheimer Res. 11, 389–398.

Liu, X., Wang, S., Zhang, X., Wang, Z., Tian, X., He, Y., 2014. Abnormal amplitude of low-frequency fluctuations of intrinsic brain activity in Alzheimer's disease. J. Alzheimer's Dis. 40, 387–397.

Love, J., Selker, R., Marsman, M., Jamil, T., Dropmann, D., Verhagen, A.J., Ly, A., Gronau, Q.F., Smira, M., Epskamp, S., Matzke, D., Wild, A., Rouder, J.N., Morey, R.D., Wagenmakers, E.-J., 2015. JASP (Version 0.7) [Computer software].

Mascali, D., DiNuzzo, M., Gili, T., Moraschi, M., Fratini, M., Maraviglia, B., Serra, L., Bozzali, M., Giove, F., 2015. Intrinsic patterns of Coupling between correlation and amplitude of low-frequency fMRI fluctuations are disrupted in Degenerative dementia mainly due to functional Disconnection. PLoS One 10, e0120988.

Mormino, E.C., Smiljic, A., Hayenga, A.O., Onami, S.H., Greicius, M.D., Rabinovici, G.D., Janabi, M., Baker, S.L., Yen, I.V., Madison, C.M., Miller, B.L., Jagust, W.J., 2011. Relationships between beta-amyloid and functional connectivity in different components of the default mode network in aging. Cereb. Cortex 21, 2399–2407.

Morris, J.C., Weintraub, S., Chui, H.C., Cummings, J., DeCarli, C., Ferris, S., Foster, N.L., Galasko, D., Graff-Radford, N., Peskind, E.R., Beekly, D., Ramos, E.M., Kukull, W.A., 2006. The uniform data set (UDS): clinical and cognitive Variables and Descriptive data from Alzheimer disease Centers. Alzheimer Dis. Assoc. Disord. 20, 210–216.

Mungas, D., Reed, B.R., Crane, P.K., Haan, M.N., González, H., 2004. Spanish and English neuropsychological assessment Scales (SENAS): further Development and psychometric characteristics. Psychol. Assess. 16, 347–359.

Pasquini, L., Scherr, M., Tahmasian, M., Myers, N.E., Ortner, M., Kurz, A., Förstl, H., Zimmer, C., Grimmer, T., Akhrif, A., Wohlschläger, A.M., Riedl, V., Sorg, C., 2016. Increased intrinsic activity of medial-temporal lobe Subregions is associated with decreased cortical Thickness of medial-parietal Areas in patients with Alzheimer's disease dementia. J. Alzheimer's Dis. 51, 313–326.

Petrella, J.R., Sheldon, F.C., Prince, S.E., Calhoun, V.D., Doraiswamy, P.M., 2011. Default mode network connectivity in stable vs progressive mild cognitive impairment. Neurology 76, 511–517.

Power, J.D., Barnes, K.A., Snyder, A.Z., Schlaggar, B.L., Petersen, S.E., 2012. Spurious but systematic correlations in functional connectivity MRI networks arise from subject motion. Neuroimage 59, 2142–2154.

Power, J.D., Mitra, A., Laumann, T.O., Snyder, A.Z., Schlaggar, B.L., Petersen, S.E., 2014. Methods to detect, characterize, and remove motion artifact in resting state fMRI. Neuroimage 84, 320–341.

Raichle, M.E., MacLeod, A.M., Snyder, A.Z., Powers, W.J., Gusnard, D.A., Shulman, G.L., 2001. A default mode of brain function. Proc. Natl. Acad. Sci. U. S. A. 98, 676–682.

Ruxton, G.D., 2006. The unequal variance t-test is an underused alternative to Student's t-test and the Mann-Whitney U test. Behav. Ecol. 17, 688–690.

Sheline, Y.I., Raichle, M.E., 2013. Resting state functional connectivity in preclinical Alzheimer's disease. Biol. Psychiatry 74, 340–347.

Smith, S.M., Fox, P.M.T., Miller, K.L., Glahn, D.C., Fox, P.M.T., Mackay, C.E., Filippini, N., Watkins, K.E., Toro, R., Laird, A.R., Beckmann, C.F., 2009. Correspondence of the brain's functional architecture during activation and rest. Proc. Natl. Acad. Sci. U. S. A. 106, 13040–13045.

Song, X.-W., Dong, Z.-Y., Long, X.-Y., Li, S.-F., Zuo, X.-N., Zhu, C.-Z., He, Y., Yan, C.-G., Zang, Y.-F., 2011. REST: a toolkit for resting-state functional magnetic resonance imaging data processing. PLoS One 6, e25031.

Weiler, M., Teixeira, C.V.L., Nogueira, M.H., de Campos, B.M., Damasceno, B.P., Cendes, F., Balthazar, M.L.F., 2014. Differences and the relationship in default mode network intrinsic activity and functional connectivity in mild Alzheimer's disease and amnestic mild cognitive impairment. Brain Connect 4, 567–574.

Whitfield-Gabrieli, S., Moran, J.M., Nieto-Castañón, A., Triantafyllou, C., Saxe, R., Gabrieli, J.D.E., 2011. Associations and dissociations between default and self-reference networks in the human brain. Neuroimage 55, 225–232.

Yu-Feng, Z., Yong, H., Chao-Zhe, Z., Qing-Jiu, C., Man-Qiu, S., Meng, L., Li-Xia, T., Tian-Zi, J., Yu-Feng, W., Zang, Y., He, Y., Zhu, C., Cao, Q., Sui, M., Liang, M., Tian, L., Jiang, T., Wang, Y., 2007. Altered baseline brain activity in children with ADHD revealed by resting-state functional MRI. Brain Dev. 29, 83–91.

Zhang, D., Raichle, M.E., 2010. Disease and the brain's dark energy. Nat. Rev. Neurol. 6, 15–28.

Zou, Q.-H.H., Zhu, C.-Z.Z., Yang, Y., Zuo, X.-N.N., Long, X.-Y.Y., Cao, Q.-J.J., Wang, Y.-F.F., Zang, Y.-F.F., 2008. An improved approach to detection of amplitude of low-frequency fluctuation (ALFF) for resting-state fMRI: fractional ALFF. J. Neurosci. Methods 172, 137–141.

Zuo, X.-N., Di Martino, A., Kelly, C., Shehzad, Z.E., Gee, D.G., Klein, D.F., Castellanos, F.X., Biswal, B.B., Milham, M.P., 2010. The oscillating brain: complex and reliable. Neuroimage 49, 1432–1445.

Zuo, X.-N., Xing, X.-X., 2014. Test-retest reliabilities of resting-state FMRI measurements in human brain functional connectomics: a systems neuroscience perspective. Neurosci. Biobehav. Rev. 45, 100–118.